JOURNAL OF APPLIED CRYSTALLOGRAPHY

Volume 52 (2019)

Supporting information for article:

Thermally Induced Transformations of Au@Cu2O Core-Shell Nanoparticles into Au-Cu Nanoparticles from Temperature-Programmed *in situ* Powder X-Ray Diffraction

Robert Koch, Guangfang Li, Shubham Pandey, Simon Phillpot, Hui Wang and Scott T. Misture

S1. Initial Precursors

Diffraction patterns and fitting of the initial precursor core-shell nanostructures at ambient conditions are shown in Fig. S1. The data is fit well using only two phases, cubic Cu_2O cuprite and FCC Au. These fits were not sensitive to Au crystallite size or cuprite strain broadening, and as such neither of these were incorporated into the fitting for these phases at any temperature. This is reasonable, as there are relatively few peaks for the cuprite phase and electron microscopy suggests that the Au crystallite diameter is about 160 nm, beyond the resolution limit of a typical laboratory powder diffraction measurements.

The core-shell nanostructures do not show significant fluctuations in atomic structure as a function of composition, with Au lattice parameters of 4.079(9) Å, consistent with that reported for bulk Au (Suh *et al.*, 1988; Wyckoff, 1963). The lattice parameter of cuprite is also consistent across all compositions at 4.250(9) Å, about 0.4% smaller than reported in the literature (Kirfel *et al.*, 1990). This suggests that the core-shell interface does exert significant strain on either lattice, a reasonable result given that the cuprite shell is not epitaxial (Zhang *et al.*, 2011), and any strain associated with lattice mismatch is likely relieved by grain boundaries within the cuprite shell.

In the core-shell systems, the average cuprite crystallite size increases the thickness of the cuprite shell, from 6.8(3) nm in the Au-rich sample to 23.4(4) nm in the Cu-rich sample, compared to 40.3(2) nm in the monometallic Cu sample. This suggests that the cuprite shell increases in thickness during synthesis through a crystal growth process rather than continuous nucleation to yield more crystallites of smaller diameter.

The twin-fault concentration in the Au core sample with no cuprite shell, at 3.53(4)%, was smaller than that refined in any of the core-shell systems. The twin-fault concentrations are similar in all three samples, with values of 4.0(2)% in the x=0.25 sample, 5.1(1)% in the x = 0.5 sample and 4.9(1)% in the x = 0.75 sample.

S2. Monometallic Reaction pathways upon heating

The composition endmembers (x = 0 and 1.0) naturally show reaction pathways that differ from the core-shell systems. *In situ* TP-PXRD data for each of the 2 monometallic systems considered are shown in Fig. S3. The pure Au system shows no chemical reaction or phase transformations at any temperature considered, as expected.

The system without Au (x = 1.0) rapidly reduces to Cu metal beginning at 140 ˚C, as in the bimetallic core-shell systems. There is no evidence of cuprite above 140 ˚C. This reduction reaction appears to occur much more quickly in pure Cu_2O than in the bimetallic core-shell system, where diffraction peaks of cuprite are apparent up 200 ˚C in some compositions. This suggests that the core-shell interface stabilizes cuprite phase, a result that warrants future investigation.

Heating the monometallic Cu system beyond the complete reduction of cuprite does lead to any additional chemical reactions or phase transformations.

S3. Monometallic crystallite size evolution upon heating

The average crystallite diameter in the monometallic Cu system is plotted as a function of temperature in Fig. S5, which shows significant crystal growth of the metallic Cu phase occurs immediately upon formation, with crystallites becoming too large to track using diffraction above 200 ˚C. This can be contrasted with the behavior of the Cu phase in the bimetallic system, where significant crystal growth was not observed. In addition, there is a noticeable decrease in the average cuprite domain size during reduction. Neither of these behaviors were observed in the bimetallic systems.

S4. Monometallic twin-fault concentration upon heating

The fraction of twin-faults for the sample containing only Au as a function of temperature in Fig. S6(A) shows a concentration of twin-faults of 3.53(4)%, lower than the core-shell systems at ambient conditions. There is no evidence of twin-fault annealing, below 100 ˚C, but annealing occurs above 100 ˚C and levels off at about 360 ˚C, to a value of ~1.4%. Fig. S6(B) shows the twin-fault fraction for the sample containing only Cu for comparison. Interestingly, the metallic Cu phase formed from reduction of cuprite appears to contain a significant concentration of twin-faults (about 5.1(4)%), which also decreases with heating, reaching ~2.5% by 360 ˚C.

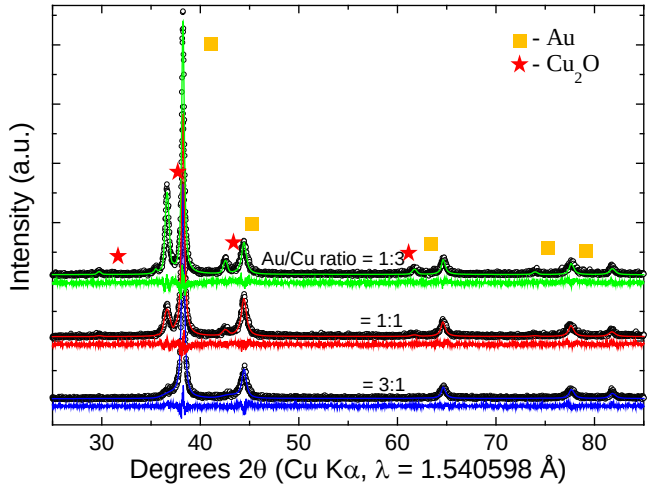

Figure S1 Powder diffraction data (black circles) for the bimetallic compositions considered here at ambient conditions. Fits are represented by overlaid colored lines, while the fit residual is shown in the same color, displaced below each XRD pattern.

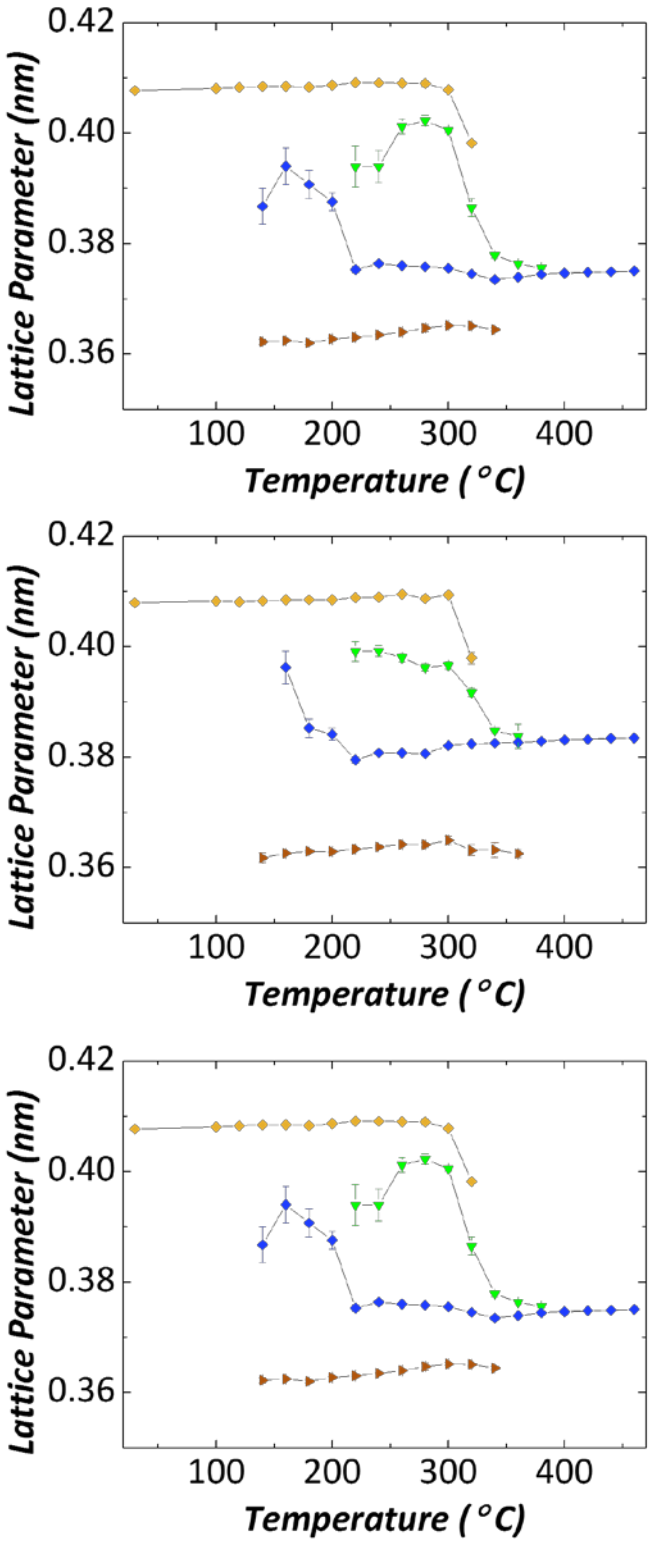

Figure S2 Refined lattice parameters of all metallic phases as a function of temperature computed using Vegard's Law for Au/Cu atomic ratios of (A) 1:3, (B) 1:1, and (C) 3:1. Error bars are present on all data points, but in some cases are smaller than the plot marker. These data were used in computing Cu atomic fraction in Fig. 2.

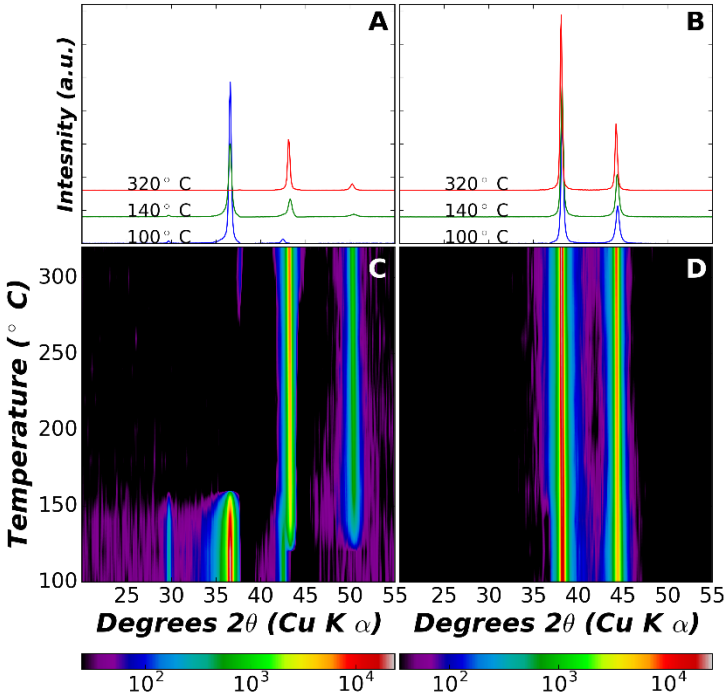

Figure S3 Logarithmic intensity maps of TP-PXRD data as a function of temperature for monometalic reactions, namely (C) Cu and (D) Au. Selected diffraction profiles at temperatures of interest are plotted above for (A) Cu and (B) Au.

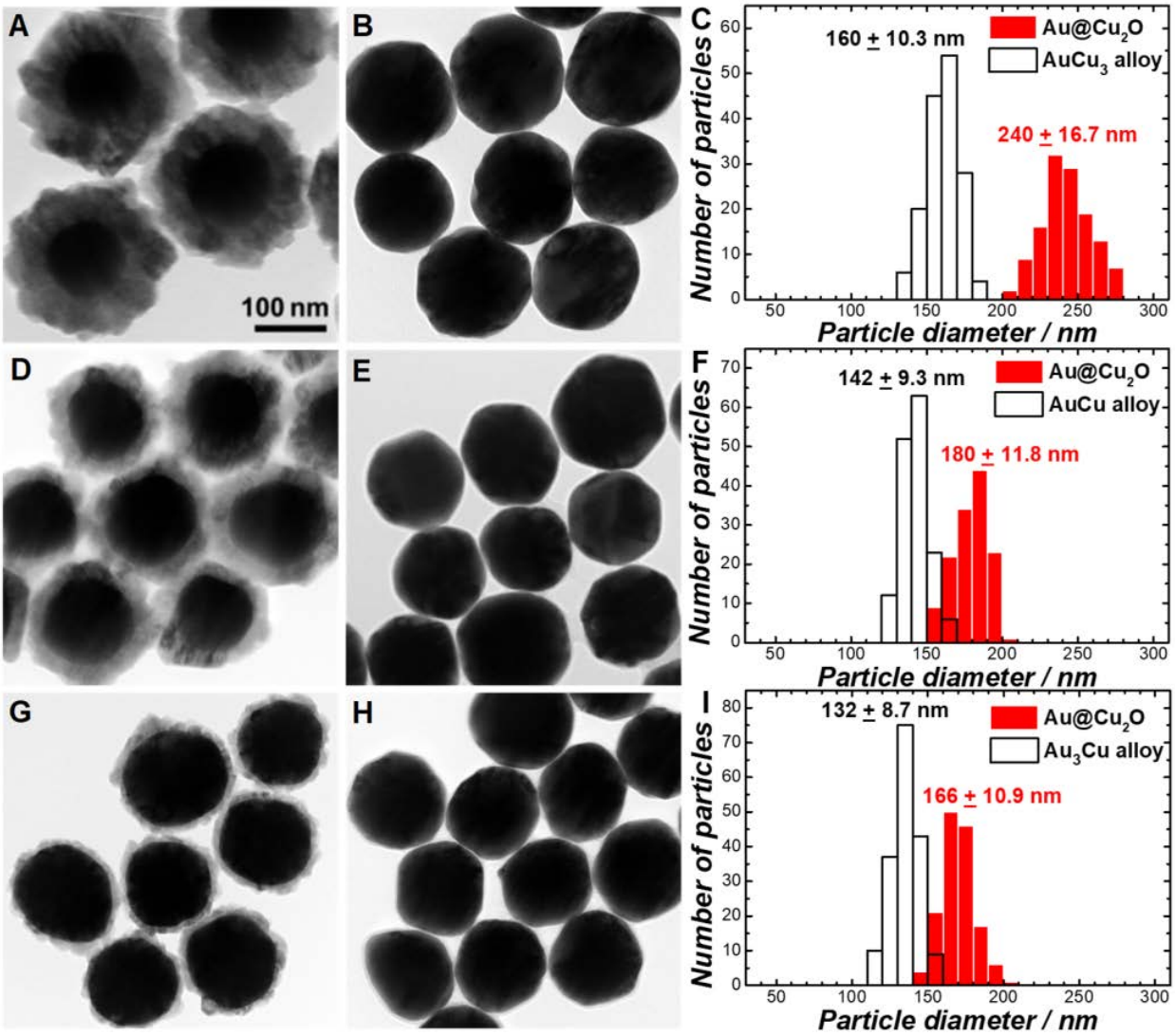

Figure S4 TEM images of (A) Au@Cu_2O core-shell nanoparticles and (B) Au-Cu alloy nanoparticles and (C) size distributions of the nanoparticles with Au/Cu atomic ratio of 1:3. TEM images of (D) Au@Cu_2O core-shell nanoparticles and (E) Au-Cu alloy nanoparticles and (F) size distributions of the nanoparticles with Au/Cu atomic ratio of 1:1. TEM images of (G) Au@Cu_2O core-shell nanoparticles and (H) Au-Cu alloy nanoparticles and (I) size distributions of the nanoparticles with Au/Cu atomic ratio of 3:1. The alloy nanoparticles were synthesized by thermally heating the Au@Cu_2O core-shell nanoparticles at 450 ˚C in flowing H_2 (50 sccm) at 100 Torr for 15 min in a tube furnace.

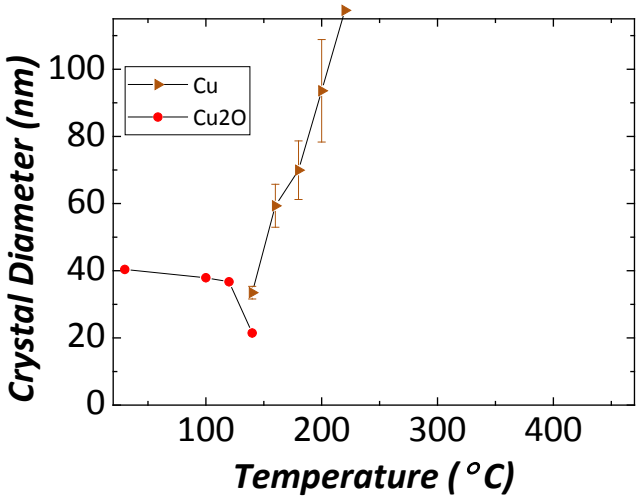

Figure S5 Average crystallite diameter for each phase as a function of temperature in the monometallic Cu reaction.

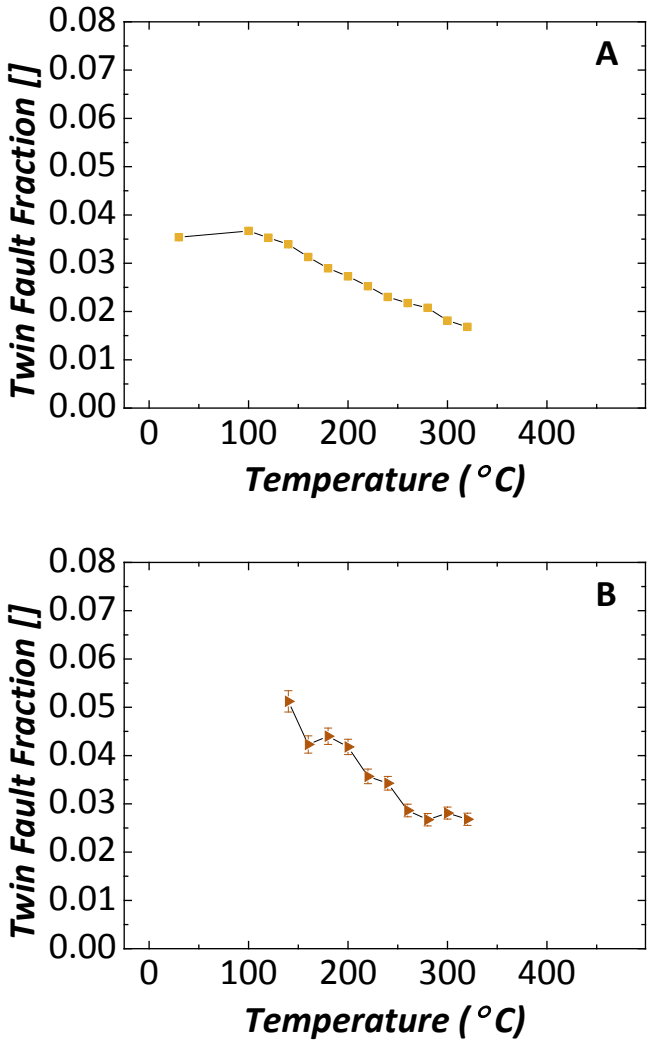

Figure S6 Twin-fault concentration as a function of temperature for the monometallic systems (A) Au and (B) Cu.

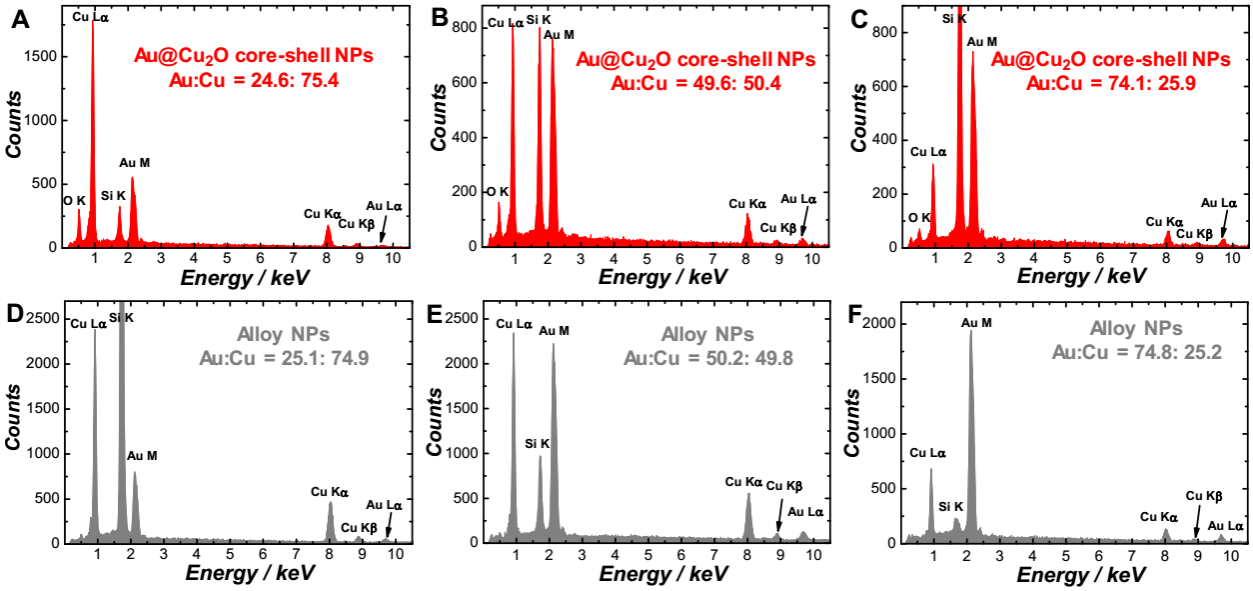

Figure S7 Energy dispersive spectra of Au@Cu_2O core-shell nanoparticles with Au/Cu atomic ratios around (A) 1:3, (B) 1:1, and (C) 3:1. Energy dispersive spectra of Au-Cu alloy nanoparticles with Au/Cu atomic ratios around (D) 1:3, (E) 1:1, and (F) 3:1.

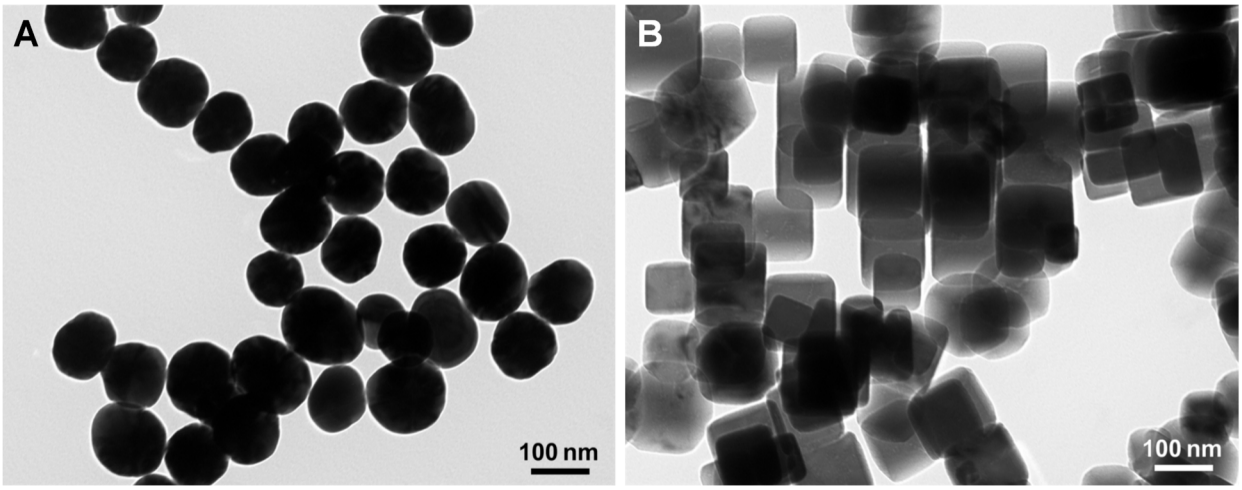

Figure S8 TEM images of (A) Au and (B) Cu_2O nanoparticles at room temperature before heating.